PII: S0032-3861(96)00817-8

Polymer Vol. 38 No. 12, pp. 3059–3068, 1997

0032-3861/97/$17.00 + 0.00

Molecular modelling and structure studies of LARC-CPI semicrystalline polyimide

Mark V. Brillhart*, Yao-Yi Cheng, Pradnya Nagarkart and Peggy Cebe‡
Department of Materials Science and Engineering, Massachusetts Institute of Technology, Cambridge, MA 02139, USA
(Received 1 August 1994; revised 26 July 1996)

Molecular modelling and X-ray structure studies were undertaken to determine the crystalline unit cell of LARC-CPI, a thermoplastic semicrystalline polyimide. We present results of a molecular mechanics based model of the energy minimized unit cell structure. The unit cell of LARC-CPI has lattice parameters of $a = 8.0$, $b = 6.0$, $c = 37.1$ Å, $\alpha = \beta = \gamma = 90°$ as determined from the model. The model unit cell contains two monomer units, one at the centre of four equivalent monomers. This gives a cell density of 1.47 g cm^{-3} which compares well with the experimentally determined unit cell density of 1.507 ± 0.2 g cm^{-3}. Fibre and powder X-ray diffraction patterns were constructed based on the model unit cell. To compare the model diffraction patterns with experimental data, a novel preparation method developed in earlier work was used to obtain highly oriented LARC-CPI films. Films recrystallized by solvent exposure at the reflux temperature had *c*-axes preferentially aligned along the film normal. The *c*-axis repeat length was determined experimentally to be 37.5 Å in agreement with the model value. X-ray photoelectron spectroscopy was used to identify the origin of a unique, radiation sensitive diffraction peak observed in some LARC-CPI films. This peak could not be indexed using the proposed model unit cell parameters. We suggest that this peak arises from oriented crystalline diamines, or diamine-terminated chains, located at the film surfaces. © 1997 Published by Elsevier Science Ltd.

INTRODUCTION

Aromatic polyimides as a result of their unique combination of properties satisfy a broad range of engineering requirements and have the potential to be employed in a multitude of service environments[1–14]. The processability of polyimides has been greatly improved by enhancing chain mobility through chemical modifications made to the diamine and dianhydride units which react to from the polymer structural repeat unit. Scientists at the NASA Langley Research Center have incorporated phenyl-ether and phenyl-ketone groups into polyimides to obtain high temperature materials that can be melt processed via thermoforming techniques[6,7,15–18].

LARC-CPI is one of the novel semicrystalline thermoplastic polyimides developed at the NASA Langley Research Center[6]. This polymer is produced by the synthesis of 3,3′,4,4′-benzophenonetetracarboxylic dianhydride (BTDA) and 1,3-bis(4-aminophenoxy-4′-benzoyl)benzene (BABB). The chemical repeat unit of LARC-CPI is:

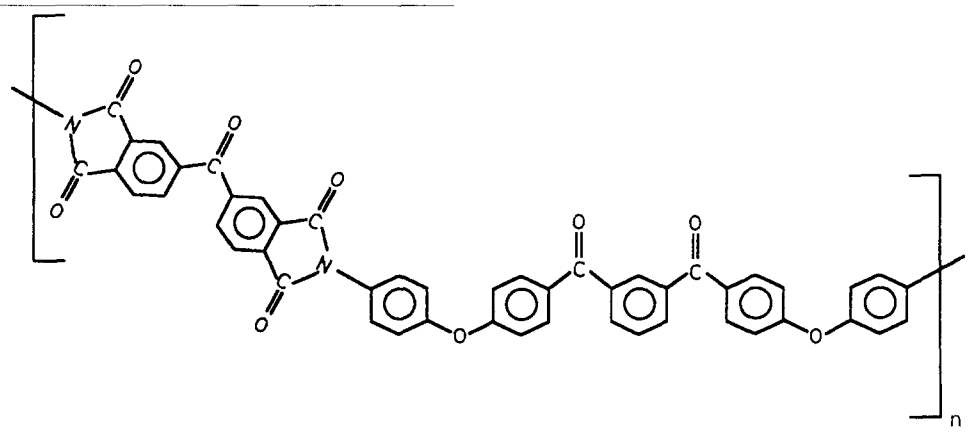

The length of the extended monomer unit was first estimated to be about 36 Å[19] using CPK models.

LARC-CPI possesses excellent thermal properties as manifested in its high glass transition ($T_g = 222°C$) and

* Present address: Bonuttti Orthopaedic Clinic, Effingham, IL 62401, USA
† Present address: Polaroid Corp., Cambridge, MA 02139, USA
‡ To whom correspondence should be addressed

melting (T_m = 355°C) temperatures measured by differential scanning calorimetry (d.s.c.)[16,20]. This polyimide also possesses excellent mechanical and adhesive properties[6,7,20–22]. Additionally, LARC-CPI has good chemical resistance[20] and a relatively low dielectric constant ($\epsilon = 3.2$[23]) and optical index of refraction (n = 1.682 to 1.700 depending on the degree of crystallinity[24].

Structural studies of LARC-CPI have been undertaken by our group and others. Transmission and scanning electron microscopy studies[25–28] along with Avrami analysis of crystallization kinetics of LARC-CPI[25,27,28] have been reported by Wilkes and the members of his research group. These researchers have also employed d.s.c., small angle (SAXS) and wide angle (WAXS) X-ray scattering, and molecular modelling to study this material[27]. Our group has reported characterization of the thermal, mechanical and electrical properties of LARC-CPI as a function of processing history and crystallinity[19,21–23]. Highly oriented zone annealed films of LARC-CPI were studied using d.s.c., WAXS and SAXS, and dynamic mechanical analysis (d.m.a.)[21,22].

Although many aspects of semicrystalline LARC-CPI have been explored, only recently had a preliminary determination of the crystalline unit cell lattice parameters been presented by our group[21,22]. Here we present results of molecular modelling and structural investigations which were undertaken to produce a more accurate model of the crystalline unit cell of LARC-CPI[29–31]. We present a molecular mechanics based model of the energy minimized unit cell structure of LARC-CPI. Validation of the model is based on comparison of simulated X-ray data with experimentally obtained results of fibre WAXS[21,22]. Calculated model unit cell densities compare very favourably to experimentally estimated values[19] providing additional support for this model. A unique reflection observed in the X-ray patterns[21,22,29] of this material is also discussed. X-ray diffraction and X-ray photoelectron spectroscopy are employed to explore the microstructural origin of this peak which is associated with orientation of diamine moieties.

EXPERIMENTAL

Solvent cast films of LARC-CPI were provided by Dr Terry St. Clair (NASA Langley Research Center). The as-received films, 0.06 mm thick, were fully crystallized and completely imidized. The degree of crystallinity of the samples was previously reported to be approximately 0.40[21]. This value was obtained from differential scanning calorimetry (d.s.c.) experiments and a heat of fusion of LARC-CPI crystals of $92 \pm 0.2\,J\,g^{-1}$ as reported by Rich *et al.*[23]. The as-received specimens were found to be unoriented based on two dimensional WAXS experiments[21].

Some of the solvent cast films were subject to boiling 1-methyl-2-pyrrolidinone (NMP) solvent to enhance crystallinity and crystalline orientation[19]. NMP treatment does not dissolve the films (no weight loss was observed after treatment) but increases the molecular mobility to permit recrystallization. Films were heated in NMP to the reflux temperature (204°C) for 18 h, then cooled and washed in water for 2 h to remove NMP. The films were placed on filter paper and dried constrained between perforated ceramic plates, under vacuum at 106°C overnight. Films prepared in this manner were highly oriented with the c-axis aligned along the normal to the film plane.

WAXS scans were performed utilizing a Rigaku RU300 diffractometer equipped with a rotating copper anode ($\lambda = 1.5$ Å) and a diffracted beam graphite monochromator. The generator operating voltage and current were 50 kV and 200 mA, respectively; 1.0 degree diffraction and scatter slits were used with a 0.15° receiving slit. 2θ was varied from 2° to 65° at $1.0°\,m^{-1}$. The step size was set to 0.02°. Silicon standard powder obtained from the National Institute of Standards and Technology was placed on the surface of selected samples to calibrate peak positions. The first silicon diffraction peak for $\lambda(CuK_\alpha)$ occurs at $2\theta = 28.44°$.

A Surface Science Instruments SSX 100 spectrometer was employed to conduct angle resolved X-ray photoelectron spectroscopy (ARX.p.s.) studies. This system produced monochromatized AlK_α X-rays at an energy of 1486.6 eV. A base pressure of better than 10^{-9} torr was maintained for all ARX.p.s. experiments. The specimen holder was capable of both tilt and rotation movements. Ejected photoelectrons were collected at a nominal take off angle (TOA) of 35° as measured from the surface of the sample film. The TOA was incrementally varied in 10° steps from 20° to 90°. This allowed for a depth profile to be obtained without resorting to sputtering. A flood gun (secondary low energy electron source) was utilized to prevent the surface of these insulating samples from charging. Phenyl carbon peaks were corrected to an energy of 285 eV and used as an internal reference for all other peaks.

MODELLING

CERIUS™ and POLYGRAF™, two commercially available software packages distributed by Molecular Simulations Inc., were employed for the modelling portion of this work. Molecular mechanics modelling was performed utilizing the Dreiding II force field and its associated parameters. Energy due to bond deformation E_b, bond angle bending E_θ and bond torsion E_ϕ were included in the energy calculations, using typical expressions[32]:

$$E_b = \frac{1}{2}K_b(R - R_o)^2 \quad (1)$$

$$E_\theta = \frac{1}{2}k_\theta(\theta - \theta_o)^2 \quad (2)$$

$$E_\phi = \sum_{n=1}^{p}\frac{1}{2}k_{\phi,n}[1 - d\cos(n\phi)] \quad (3)$$

Here θ and R denote bond angles and bond lengths with the subscript o indicating the equilibrium value. k_b, k_θ and k_ϕ are the Dreiding II force field constants[32]. The bond torsion angle is denoted by the variable ϕ, p is the periodicity of the nth energy barrier, n is the periodic peak or well number, and d is a constant that is employed to set either planar *trans* or *cis* as the minimum barrier value.

Coulombic (E_c) and Van der Waals (E_{vdw}) energies were also included when determining the overall energy of a system. Typical expressions for these energies are[32]:

$$E_c = C_o\sum_{i>j}^{p}\frac{Q_iQ_j}{\epsilon R_{ij}} \quad (4)$$

$$E_{vdw} = \frac{A}{R^{12}} - \frac{B}{R^6} = D_o\left[\left(\frac{R_o}{R}\right)^{12} - 2\left(\frac{R_o}{R}\right)^6\right] \quad (5)$$

Here ϵ is the dielectric constant, Q_i and Q_j are partial charges and R_{ij} is the distance between atoms. C_o is a conversion factor employed to yield Coulombic interaction energy in units of kcal mol^{-1}. D_o is the maximum finite bond energy and R_o is the interatomic distance at which the bond energy is equal to D_o. R is the actual distance between the atoms in question.

Detailed discussion of molecular mechanics[32–35] and the Dreiding II force field[36] can be found in the literature. This force field, along with others, has been used extensively and describes a wide range of atomic configurations and interactions quite well[37–42]. To employ Coulombic interactions, partial charges were calculated via the charge equilibration method developed by Rappe and Goddard[43].

The modelling of the crystal structure of LARC-CPI consisted of our stages. First the conformation of the most probable crystal repeat unit was determined by performing a Monte Carlo search procedure on oligomers of LARC-CPI. Over 250 pentamer conformations were generated and a crystal repeat unit was selected based on both energetic and physical criteria. A pentamer was subject to the Monte Carlo search to minimize the effects of free ends on the most probable conformation of the crystal repeat unit. The centre structural unit of the pentamer was extracted and used to construct the crystal repeat unit. Small modification of the torsion angles was then used in order better to meet the experimental requirements of the *c*-axis repeat unit.

Second, it was necessary to determine the crystalline unit cell type. The unit cell lattice parameters were roughly approximated based on our previous estimates of the lattice parameters of LARC-CPI[21]. Once model unit cells were obtained, simulated X-ray patterns were made and compared to experimental data[21,22]. Crystal density for each model unit cell was calculated and compared to the experimental value of crystal lattice density.

The third step was to obtain the unit cell lattice parameters by incrementally varying *a* and *b* lattice parameters and performing molecular mechanics minimizations and obtaining simulated X-ray and density data for each lattice parameter combination. Candidate model unit cells were again evaluated based on comparisons of simulated and experimental data as well as consideration of the minimized unit cell energy. Fourth, final refinements of the model were made by examining the effects of chain setting angles and translations within the unit cell on the relative intensity distribution of simulated one dimensional X-ray patterns.

RESULTS AND DISCUSSION

Modelling the unit cell structure of LARC-CPI

The Monte Carlo search technique was employed to explore different potential unit cell repeat units. *Figure 1* contains the most probable unit cell repeat unit of LARC-CPI obtained. The heterocyclic rings of the dianhydride component are non-coplanar as a result of the benzophenone group, in contrast with other polyimides such as Kapton™ and Regulus™ New-TPI which have not rotatable bonds in the dianhydride unit.

Figures 2a–c contain the *a–b*, *a–c*, and *b–c* projections, respectively, of the model unit cell of LARC-CPI. *Figure 2d* shows the disposition of the corner and centre chains of the unit cell. The unit cell of LARC-CPI has lattice parameters of $a = 8.0$ Å, $b = 6.0$ Å, $c = 37.1$ Å, $\alpha = \beta = \gamma = 90°$. The model unit cell contains two monomer units, one in the centre of four adjacent monomers. Equivalent atom positions on the centre and corner chains are found at positions $x\ y\ z$ and $-x + \frac{1}{2}\ y + \frac{1}{2}\ -z + \frac{2}{3}$. This results in a centre chain that is rotated relative to the corner chains about the *a*- and *c*-axes. This positioning of the centre chain relative to the corner chains was also found in another semicrystalline polyimide, NEW-TPI, studied by Okuyama *et al.*[44].

An experimental pattern of a zone annealed sample of LARC-CPI is shown in *Figure 3*[21], with fibre axis vertical. Zone annealing was performed following the procedure of Kunugi[45] and Takayanagi[46]. Details of the zone drawing process and WAXS experiments have been presented[21,22]. The pattern in *Figure 3* is a composite of two different exposures of the same sample. The inner rectangle was exposed to reveal the meridional reflections. The outer portions of *Figure 3* were exposed for a longer time to reveal weaker quadrantal refections. The reflections used in lattice parameter determination are marked. The two theta positions, *d*-spacings, and Miller indices are summarized in *Table 1*.

Peak positions had larger uncertainty when taken from the flat film pattern of zone-drawn fibre. Because of

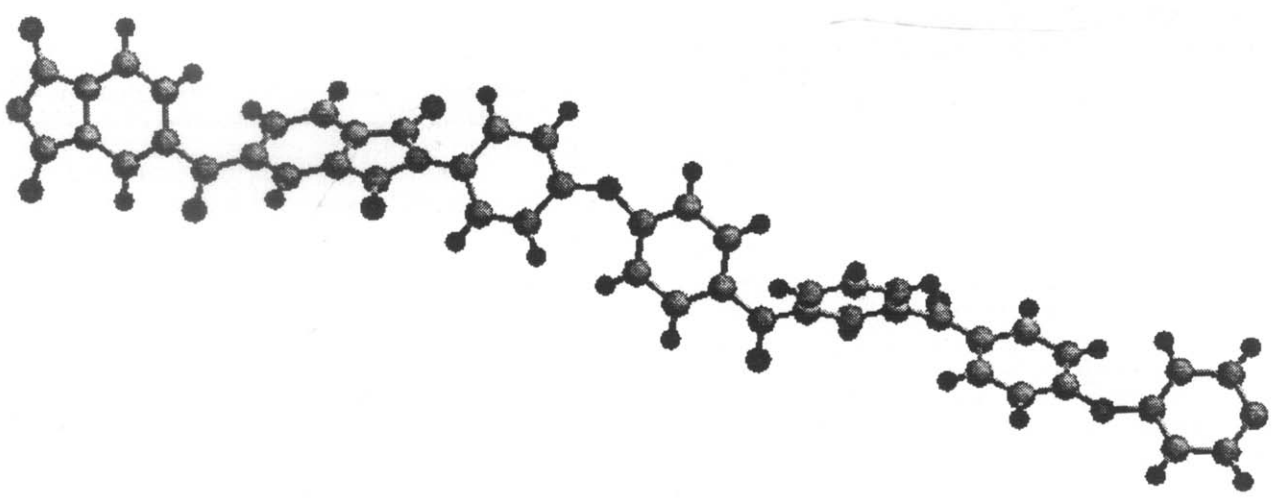

Figure 1 Most probable monomer repeat unit of LARC-CPI

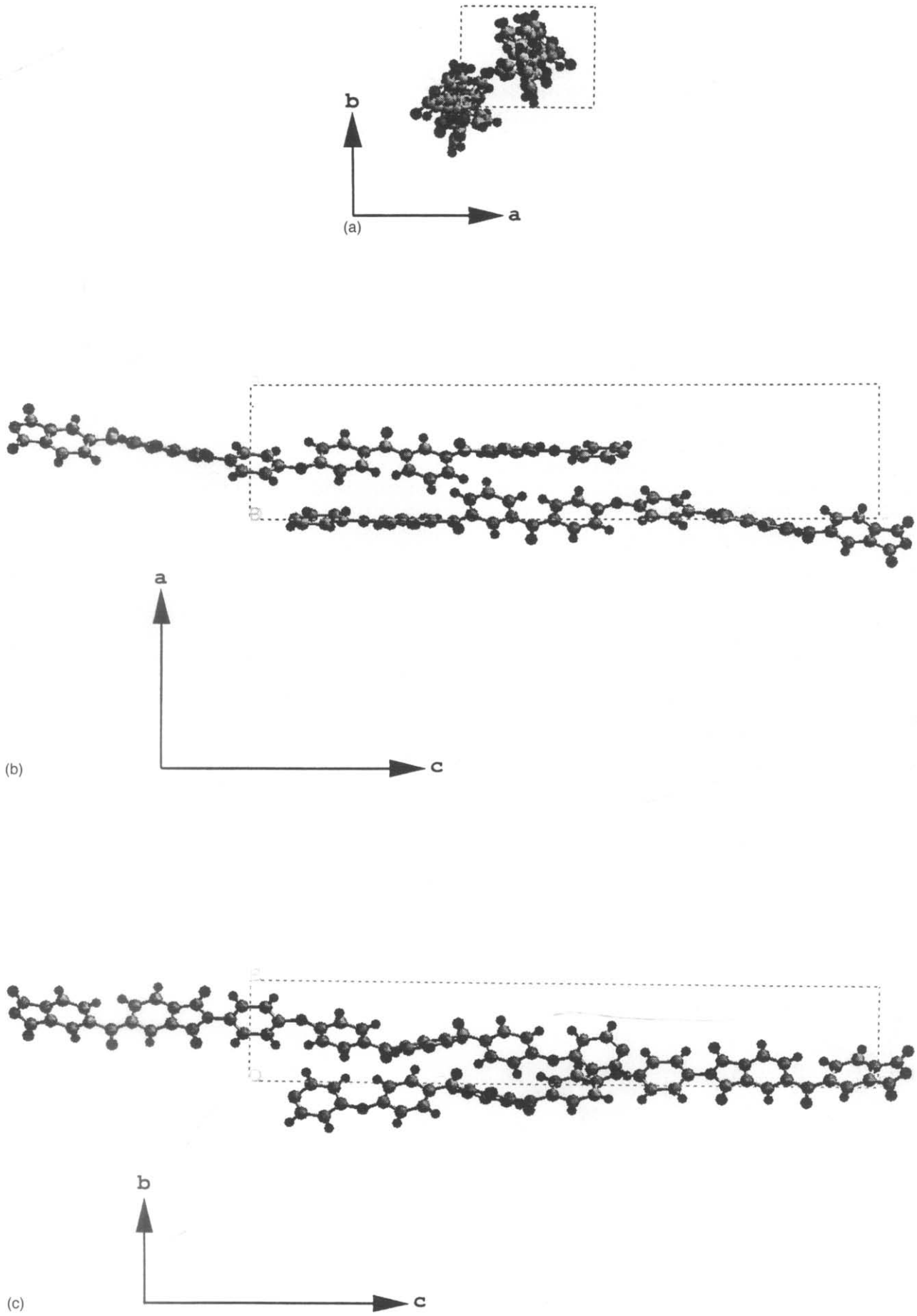

Figure 2 Projection of model unit cell of LARC-CPI in the: (a) *a–b* plane; (b) *a–c* plane; (c) *b–c* plane. (d) Disposition of the corner and centre chains of the unit cell

the very large *c*-axis repeat distance there is crowding of intense (*hkl*) reflections with low *l* near the equator. Thus, it was experimentally difficult to resolve these reflections; several of this type were seen as broad arcs, with diffracted intensity contributions from more than one set of lattice planes. In addition, reflections (001) and (002) were obscured by the beam stop and cannot be seen in *Figure 3*. When a larger sample-to-detector distance was used to reveal (001) and (002), the silicon calibration standard could not be simultaneously seen. Thus, the *c*-axis had a larger experimental uncertainty and lead to preliminary predictions of a slightly shorter *c*-axis repeat length[29–31].

We have recently produced highly oriented LARC-CPI films with the correct orientation to be examined in $\theta/2\theta$ reflection mode WAXS[19,47]. To obtain a highly oriented sample, we used the NMP solvent exposure treatment described in the Experimental section which had been developed in our laboratory in earlier work[19,47]. Films prepared this way were oriented with their *c*-axis preferentially aligned along the normal to the film plane. The WAXS scan of NMP treated LARC-CPI is shown in *Figure 4*, in which many reflections of the type (00*l*) can be seen. We determined the *c*-axis repeat distance more accurately from the slope of a plot of:

$$l = d_{00l}\ 2\sin\theta_{00l}/\lambda \qquad (6)$$

where *l* is the peak index number, θ is the half-scattering angle, and λ is the X-ray wavelength. The *c*-axis repeat found by this method is 37.5 ± 0.02 Å.

Table 1 contains the angular positions (2θ at $\lambda = 1.54$ Å) and *d*-spacings of selected reflections of the model and experimental patterns shown in *Figure 3* and *4*. The subscript m denotes model, f denotes the experimental pattern (*Figure 3*), and s denotes the experimental pattern from the solvent exposed sample (*Figure 4*).

Figure 5a shows the model one-dimensional diffraction (powder type) pattern over the 2θ range from 0 to 40°. The model assumes that there is an isotropic crystal orientation distribution when simulating one dimensional patterns. There is also no amorphous halo contribution included in the simulated powder pattern. Peak broadening in the simulation occurs as a result of (an arbitrarily chosen) crystal size effect. *Figure 5b* shows a typical one dimensional diffraction pattern for a stack of three films of unoriented, as-received LARC-CPI in $\theta/2\theta$ reflection mode. One sharp silicon peak is labelled and used as a reference for determining positions of other peaks. Four crystalline reflections are superimposed on the amorphous halo, and are numbered for discussion purposes. Amorphous halo subtraction was made when determining the experimental peak positions. Tabulated *d*-spacings and 2θ values for the model and experimental one dimensional data are listed in *Table 2*.

Structural investigations

In this section we discuss several aspects of LARC-CPI structure that were identified in light of the crystalline unit cell model proposed in the prior section. These include crystal lattice density and formation of oriented diamines in pristine solvent cast films.

Previous attempts have been made at modelling the crystalline region of LARC-CPI[27]. In this model the simulated density of the crystalline lattice of LARC-CPI was reported to be $0.4\,g\,cm^{-3}$ which is a physically unrealistic value. Measurements of bulk density of LARC-CPI films made in our laboratory indicated that amorphous material had a density of $1.335\,g\,cm^{-3}$ while the density of semicrystalline films ranged from 1.343 to $1.376\,g\,cm^{-3}$ [19]. Combining density measurements with degree of crystallinity determined from WAXS, Friler obtained an extrapolated crystal lattice density of $1.507 \pm 0.02\,g\,cm^{-3}$ [19]. Our model yielded a simulated crystal density of $1.47\,g\,cm^{-3}$. Thus the model proposed in this work is in excellent agreement with both experimentally obtained X-ray and density data.

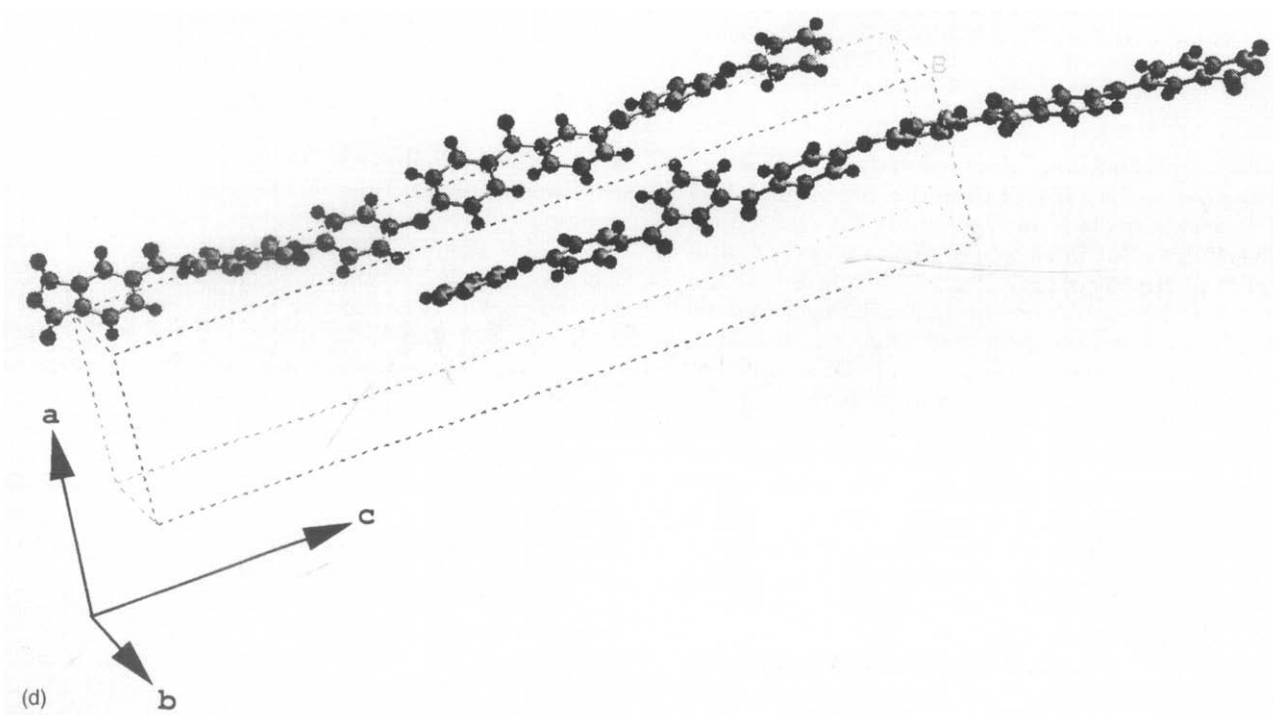

Figure 2 Continued

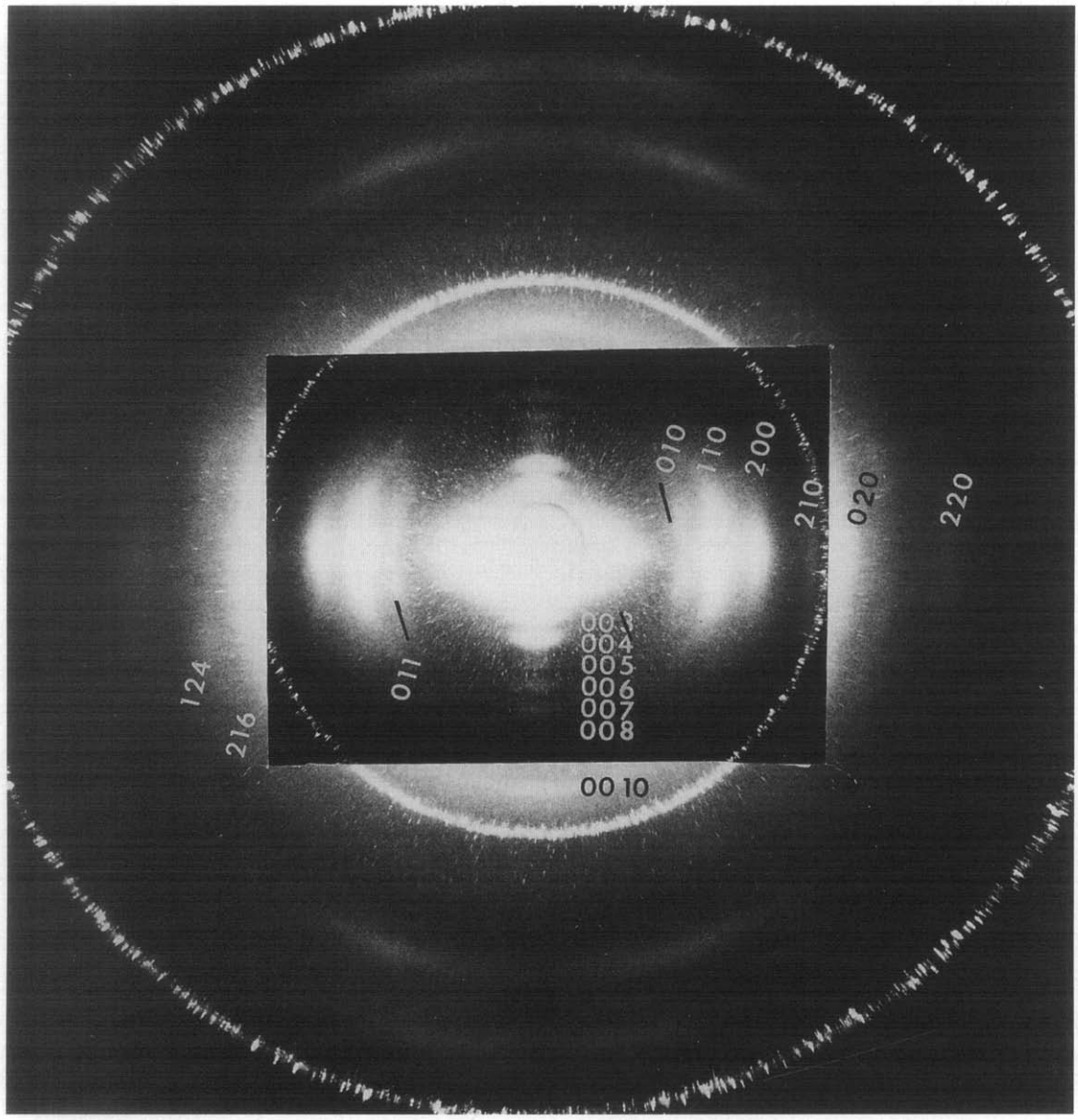

Figure 3 Experimental fibre X-ray diffraction pattern of LARC-CPI zone annealed film[21]. The figure is a composite of two different exposures. The inner rectangle was exposed to reveal meridional reflections, while the outer portions of the pattern were exposed to reveal weak quadrantal reflections. Spotty rings are from silicon used as a calibration standard

A unique reflection was observed in the WAXS scans of some pristine LARC-CPI films (i.e. films which had never been exposed to X-ray radiation). This reflection, marked as Peak A, can be seen in *Figure 6*, curve 1, at a *d*-spacing of approximately 25.2 Å. This peak is sharp and intense, but could not be indexed to any set of lattice planes using the proposed unit cell structure. Upon rotating the specimen 90° about an axis normal to the surface of the sample and re-scanning, this reflection vanished. When the specimen was remounted in the position used to obtain *Figure 6*, curve 1, and re-scanned the peak reappeared but at a much lower intensity as shown in *Figure 6*, curve 2. Peak A at 25.2 Å is highly radiation sensitive, and possibly also sensitive to film orientation. The intensities of the crystal reflections increased slightly after the two films rotation and repeated X-ray exposure.

The same reflection at a *d*-spacing of 24.5 ± 1.4 Å was observed by Teverovsky[21] in two-dimensional fibre patterns of zone annealed LARC-CPI. The data reported by Teverovsky were obtained on a different X-ray system (Philips PW1830 generator) than the one employed to obtain *Figure 6* and used a different X-ray technique (flat film WAXS using a Statton camera) in which the sample was subjected to an 18 h X-ray exposure. The 24.5 Å reflection appeared on the meridian of the fibre patterns, with an intensity weaker than either the 001 or 002 reflections[21].

An X-ray examination of this peak focused on X-ray sensitivity. A fresh sample with no prior exposure to X-radiation was scanned twice in succession. Peak A intensity decayed dramatically from the first to the second scan; no other peak intensities were affected. The fact that Peak A intensity decayed significantly upon exposure may explain why no other higher order peaks were observed of similar width and intensity.

ARXPS experiments were conducted to explore the origin of this unique reflection. Since Peak A was not described by the model and was the only radiation sensitive peak in the pattern it is due to some ordered structure that is independent of the unit cell of LARC-CPI. *Figure 7* shows typical results of ARX.p.s. experiments.

Table 1 Miller indices (*hkl*), scattering angle, 2θ, and *d*-spacing for LARC-CPI determined from the model fibre pattern (m), from experimental fibre data (f), and from experimental data on solvent treated films (s), X-ray wavelength was 1.54 Å

hkl_m	$2\theta_m$ (degrees)	d_m (Å)	$2\theta_f$ [a] (degrees)	d_f [a] (Å)	$2\theta_s$ (degrees ±0.05)	d_s (Å ±0.015)
001	2.4	37.1	24.4 ± 0.2	36.6 ± 3	—	—
002	4.8	18.54	4.9 ± 0.2	18.0 ± 0.8	—	—
003	7.2	12.36	7.4 ± 0.3	11.9 ± 0.5	7.22	12.23
004	9.5	9.27	9.5 ± 0.3	9.3 ± 0.3	9.26	9.54
005	11.9	7.41	12.4 ± 0.3	7.1 ± 0.2	11.98	7.38
006	14.3	6.18	14.5 ± 0.3	6.1 ± 0.1	14.18	6.24
007	16.7	5.30	16.8 ± 0.3	5.3 ± 0.1	16.56	5.35
008	19.2	4.63	19.2 ± 0.3	4.6 ± 0.1	18.46	4.80
0010	24.0	3.71	24.3 ± 0.3	3.66 ± 0.6	23.82	3.73
0013	31.4	2.85	—	—	31.12	2.87
0014	33.8	2.65	—	—	33.52	2.67
010	14.8	6.0	15.0 ± 0.3	5.9 ± 0.1	—	—
011	14.94	5.92	15.2 ± 0.4	5.8 ± 0.2	—	—
110	18.5	4.80	18.5 ± 0.3	4.8 ± 0.1	18.46	4.80
200	22.2	4.00	22.1 ± 0.3	4.02 ± 0.07	—	—
210	26.8	3.33	27.1 ± 0.3	3.29 ± .05	—	—
216	30.5	2.93	29.7 ± 0.3	3.00 ± .03	—	—
020	29.7	3.0	29.9 ± 0.7	2.98 ± .07	—	—
124	33.3	2.69	32.7 ± 0.3	2.74 ± .03	—	—
220	37.4	2.40	36.7 ± 0.3	2.45 ± .02	—	—

[a] Data taken from ref. 21
— Reflection was not seen under this experimental condition

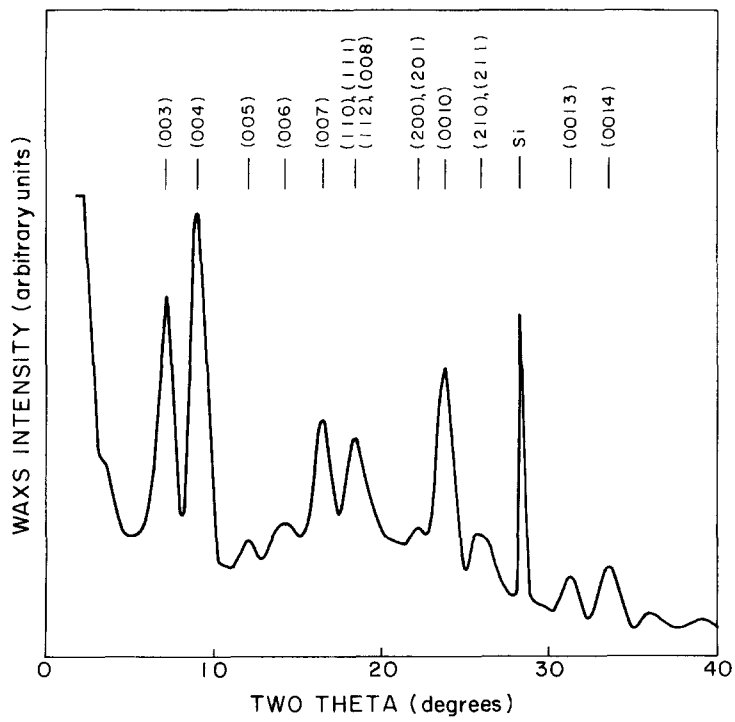

Figure 4 Experimental X-ray diffraction pattern of LARC-CPI films crystallized by solvent exposure in NMP, in $\theta/2\theta$ reflection mode

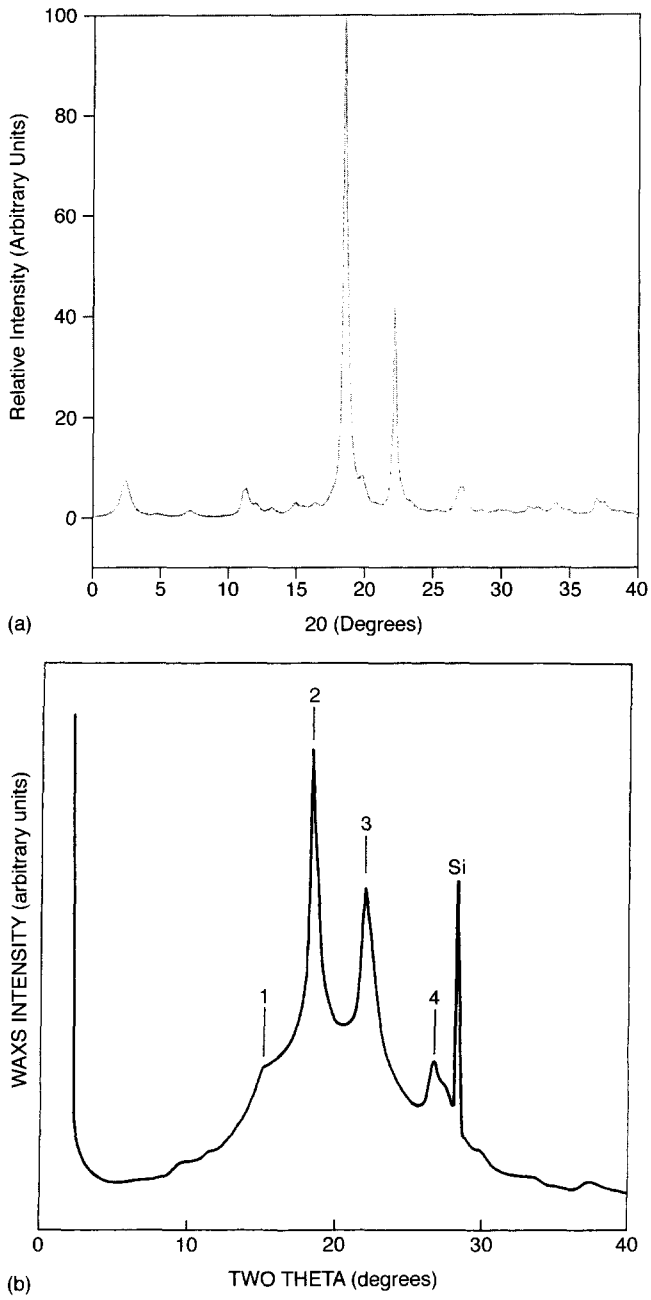

Figure 5 (a) Simulated powder X-ray diffraction pattern of LARC-CPI based on the proposed model. (b) Experimental X-ray diffraction pattern of unoriented films of LARC-CPI in $\theta/2\theta$ reflection mode. Two silicon peaks are marked

Here the percentage of carbon in carbonyl groups is shown *versus* integrated depth from the film surface. Experimentally obtained data points are indicated by solid icons. Theoretical values of percentage carbon in carbonyl are also shown in *Figure 7*, as solid lines, based on stoichiometric considerations for the diamine and dianhydride that react to form LARC-CPI, and for the polymer repeat units as a whole. The amount of carbon in carbonyl determined experimentally by ARX.p.s. lies very close upon the assumed concentration within the diamine unit. Two spots were examined on each side of the film, and similar results were obtained. There was no difference between the sides of the film, even though one side was originally against the glass casting plate and the other side was exposed to air.

From ARX.p.s. studies, we suggest that there is an excess diamine concentration at both surfaces of the film

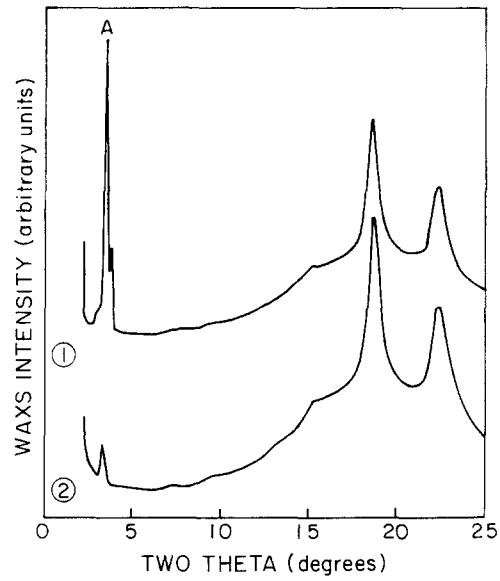

Figure 6 Experimental X-ray diffraction pattern of LARC-CPI films in $\theta/2\theta$ reflection mode, showing a unique reflection at 24.5 Å, marked as Peak A. Curve 1, first scan; curve 2, third scan of the same films after rotation by $+90°$ and $-90°$

Table 2 Miller indices (*hkl*), scattering angle, 2θ, and *d*-spacing for LARC-CPI determined from the model powder pattern (m) and from experimental powder type data (e), X-ray wavelength was 1.54 Å

Peak number[a]	*hkl*	$2\theta_m$ (degrees)	d_m (Å)	$2\theta_e$ (degrees ± 0.05)	d_e (Å ±0.015)
1[b]	011	15.0	5.92	15.3	5.79
	012	15.5	5.71		
2[b]	110	18.5	4.80	18.6	4.77
	111	18.6	4.76		
3	200	22.2	4.00	22.4	3.97
4	212	27.2	3.28	27.4	3.25

[a] Peak number corresponds to *Figure 5b*
[b] Peak intensity reflects overlap of multiple sets of planes

being examined. Thus it is possible that free diamines and/or diamine terminated chain ends are ordering and forming a (possibly crystalline) structure that is producing peak A. In order to explore the diamine ordering concept further, a molecular mechanics simulation was undertaken. A free diamine was allowed to minimize and adopt a final unperturbed conformation. The end to end length of this unit was 25.6 Å which is quite close to the *d*-spacing (25.2 Å) of Peak A.

CONCLUSIONS

A model of the crystal structure of LARC-CPI has been produced by molecular mechanics techniques. The unit cell of LARC-CPI has two chains per cell, with lattice parameters of $a = 8.0$, $b = 6.0$, $c = 37.1$ Å, $\alpha = \beta = \gamma = 90°$. The crystal lattice density is $1.47\,g\,cm^{-3}$, which agrees well with the experimental crystal density of $1.507\,g\,cm^{-3}$ [19]. Angle resolved X.p.s. results indicate there is a high concentration of diamines and/or diamine-terminated polymer molecules at both surfaces of pristine solvent cast films. These diamines form ordered structures which are highly radiation sensitive.

ACKNOWLEDGEMENTS

This research was supported by the Electric Power Research Institute, RP:8007-13. The authors thank Dr

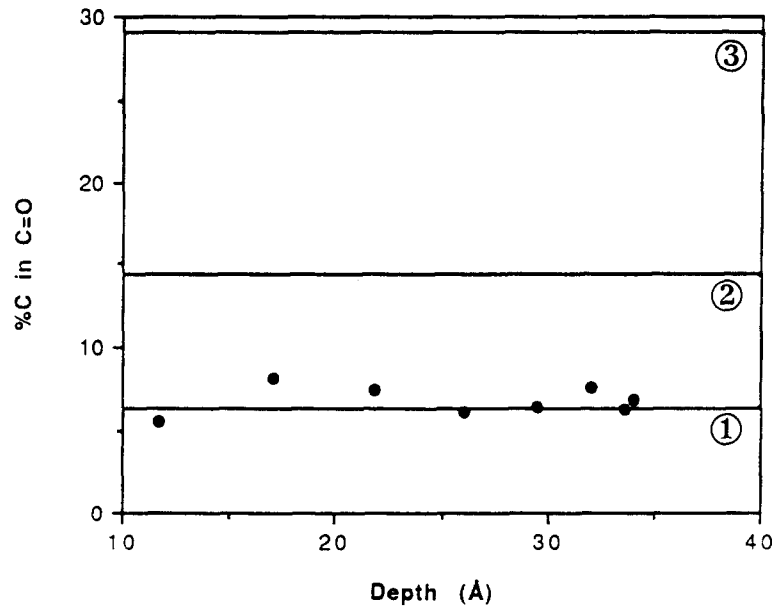

Figure 7 Angle resolved X-ray photoelectron spectroscopy results for LARC-CPI films, indicating percent carbon in carbonyl as a function of depth from the film surface (O). Solid lines indicated expected percentage carbon in carbonyl form stoichiometric considerations, for diamine (curve 1), monomer repeat unit (curve 2), and dianhydride (curve 3)

Terry St. Clair of NASA Langley for LARC-CPI films. PPG Industries Foundation is acknowledged for supporting acquisition of the Silicon Graphics Workstation used for molecular modeling studies. MVB thanks the NASA Graduate Research Program for a graduate student fellowship during a portion of this study.

REFERENCES

1. Scroog, C. E., *Macromolecular Review, Journal of Polymer of Science*, 1976, **11**, 161.
2. Critchley, J. P., Knight, G. J. and Wright, W. W., *Heat Resistant Polymers*. Plenum Press, New York, 1986, p. 200.
3. Tummala, R., Keyes, R., Grobman, W. and Kapur, S., Thin-film packaging, in *Microelectronics Packaging Handbook*, ed. R. Tummala. Van Nostrand Reinhold, New York, 1989, p. 673.
4. Arnold, C., *Macromolecular Review Journal of Polymer Science*, 1979, **14**, 265.
5. St. Clair, A. K. and St. Clair, T. L., in *Polymers for High Technology, Electronics and Photonics*, ACS Symp. Ser. 346, ed. M. J. Bowden and S. R. Turner. American Chemical Society, Washington, DC, 1987, p. 437.
6. Hergenrother, P. M., Wakelyn, N. T. and Havens, S. J., *Journal of Polymer Science*, 1987, **25**, 1093.
7. Hergenrother, P. M. and Havens, S. J., *Journal of Polymer Science*, 1989, **27**, 1161.
8. Brekner, M. J. and Geger, C. J., *Journal of Polymer Science*, 1987, **25**, 2005.
9. Mittal, K. L. (ed.), *Polyimides: Synthesis, Characterization and Applications*. Proceedings of the First Technical Conference on Polyimides, Ellenville, New York, 1983. Plenum Press, New York, 1984.
10. Webber, W. D. and Gupta, M. R. (ed.), *Recent Advances in Polyimide Science and Technology*. Proceedings of the Second Technical Conference on Polyimides, Ellenville, New York, 1985. SPE, Inc., Poughkeepsie, New York, 1987.
11. Geger, C., Khojasteh, M. M. and McGarth, J. E. (ed.), *Polyimides: Materials, Chemistry and Characterization*. Proceedings of the Third Technical Conference on Polyimides, Ellenville, New York, 1988. Elsevier, Amsterdam, 1989.
12. Harris, F. W., in *Polyimides*, ed. D. Wilson, H. Stenzenberger and P. Hergenrother. Chapman and Hall, New York, 1990, p. 1.
13. Senturia, S. D., in *Polymers for High Technology, Electronics and Photonics*, ACS Symp. Ser. 346, ed. M. J. Bowden and S. R. Turner. American Chemical Society, Washington, DC, 1987, p. 428.
14. Verbickey Jr., J. W. Polyimides in *Encyclopedia of Polymer Science and Engineering*, ed. Herman F. Mark. John Wiley and Sons, New York, 1987.
15. Hergenrother, P. M., *Polymer Journal*, 1987, **19**(1), 73.
16. St. Clair, T. L. and St. Clair, A. K., *Journal of Polymer Science, Polymer Chemistry*, 1977, **15**(6), 1529.
17. St. Clair, T. L., Gerber, M. K. and Gautreaux, C. R., *Polymer Material Science and Engineering*, 1989, **60**, 183.
18. St. Clair, T. L., Burks, H. D., Wakelyn, N. T. and Hou, T. H., *American Chemical Society Polymer Preprints*, 1987, **28**(1), 90.
19. Friler, J. B. M.S. Thesis, Massachusetts Institute of Technology, 1991.
20. Hergenrother, P. M., *SPE Conference on High Temperature Polymers and Their Uses*, Cleveland, OH, 2–4 October 1989.
21. Teverovsky, J. B. M.S., Thesis, Massachusetts Institute of Technology, 1993.
22. Teverovsky, J. B., Rich, D. C., Aihara, Y. and Cebe, P., *Journal of Applied Polymer Science*, 1994, **54**, 497.
23. Rich, D. C., Huo, P. P., Liu, C. and Cebe, P., *American Chemical Society, Polymer Material Science and Engineering*, 1993, **68**, 124.
24. Rich, D. C., Cebe, P. and St. Clair, A. K., *SPE ANTEC*, 1994, **40**(2), 2170.
25. Mullerleile, J. T., Risch, B. G., Brandom, D. K. and Wilkes, G. L., *American Chemical Society Polymer Preprints*, 1992, **33**(1), 409.
26. Mullerleile, J. T., Wilkes, G. L. and York, G. A., *Polymer Communications*, 1991, **32**(6), 176.
27. Mullerleile, J. T., Risch, B. G., Rodrigues, D. E. and Wilkes, G. L., *Polymer*, 1993, **34**(4), 789.
28. Mullerleile, J. T. and Wilkes, G. L., *American Chemical Society Polymer Preprints*, 1990, **3**(2), 637.
29. Brillhart, M. V., Teverovsky, J. B., Nagarkar, P. and Cebe, P., *Material Research Society Symposium Proceedings*, 1994, **323**, 251.
30. Brillhart, M. V., Teverovsky, J. B., Friler, J. B. and Cebe, P., *SPE ANTEC*, 1994, **40**(2), 1469.
31. Brillhart, M. V. M.S., Thesis, Massachusetts Institute of Technology, 1994.
32. CERIUS^{TM} Version 3.2 Updated Software Manual (1993) from Molecular Simulations Inc.
33. POLYGRAF^{TM} Version 3.0 Tutorial (1992) from Molecular Simulations Inc.
34. POLYGRAF^{TM} Version 3.0 Reference Manual (1992) from Molecular Simulations Inc.
35. SYBYL^{TM} Version 6.0 Theory Manual (1992) from TRIPOS Associates Inc.
36. Mayo, S. L., Olfason, B. D. and Goddard III, W. A., *Journal of Physical Chemistry*, 1990, **94**, 8897.
37. Fan, C. F. and Hsu, S. L., *Macromolecules*, 1991, **24**, 6244.
38. Yang, X. and Hsu, S .L., *Macromolecules*, 1991, **24**, 6680.
39. Nitzsche, S. A., Wang, Y. K. and Hsu, S. L., *Macromolecules*, 1992, **25**, 2397.
40. Li, Y. and Mattice, W. L., *Macromolecules*, 1992, **25**, 4942.

41. Clough, S. B., Sun, X. F., Tripathy, S. K. and Baker, G. L., *Macromolecules*, 1991, **24**, 4264.
42. Fan, C. F., Olafson, B. D., Blanco, M. and Hsu, S. L., *Macromolecules*, 1992, **25**, 3667.
43. Rappe, A. K. and Goddard III, W. A., *Journal of Physical Chemistry*, 1991, **95**, 3358.
44. Okuyama, K., Salaitani, H. and Arikawa, H., *Macromolecules*, 1994, **25**, 7261.
45. Kunugi, T., Akiyama, I. and Hashimoto, M., *Polymer*, 1982, **23**, 1193.
46. Kamezawa, M., Yamada, K. and Takayanagi, M., *Journal of Polymer Science*, 1979, **24**, 1227.
47. Brillhart, M. V. and Cebe, P., *Journal of Polymer Science, Polymer Physics Edition*, in press.
48. Friler, J. B. and Cebe, P., *Polymer Engineering Science*, 1993, **33**(10), 587.